EUCLID's near infrared spectro-photometer ready for flight: review of final performances

E. Medinaceli, L. Valenziano, N. Auricchio, E. Franceschi, F. Gianotti, P. Battaglia, R. Farinelli, A. Balestra, S. Dusini, C. Sirignano, et al.

EUCLID's Near Infrared Spectro-Photometer ready for flight - review of final performances

Medinaceli E.[a], Valenziano L.[a], Auricchio N.[a], Franceschi E.[a], Gianotti F.[a], Battaglia P.[a], Farinelli R.[a], Balestra A[b], Dusini S.[c], Sirignano C.[c], Borsato E.[c], Stanco L.[c], Renzi A.[c], Troja A.[c], Gabarra L.[c], Ligori S.[d], Capobianco V.[d], Corcione L.[d], Bonino D.[d], Sirri G,[e], Patrizii L.[e], Tenti M.[e], Di Ferdinando D.[e], Valieri C.[e], Mauri N.[e], Giacomini F.[f], Le Mignant D.[g], Prieto E.[g], Carle M.[g], Ducret F.[g], Gillard W.[h], Secroun A.[h], Maciaszek T.[i], Ferriol S.[j], Barbier R.[k], Grupp F.[l], Holmes W.[m], Pniel M.[m], Waczynski A.[m], Prado S.[m], Seiffert M.[m], Jhabvala M.[m], Laureijs RJ.[n], Racca G.[n], Salvignol JC.[n], Boenke T.[n], and Strada P.[n]

[a]INAF-Osservatorio di Astrofisica e Scienza dello Spazio, Via Gobetti 5, Bologna, Italy
[b]INAF-OAPd, Vicolo dell'Osservatorio 5, Padova, Italy
[c]INFN-Pd, Via marzolo 8, Padova, Italy
[d]INAF-OATo, Pino Torinese, Torino, Italy
[e]INFN-Bo, Viale B. Pichat 6/2, Bologna, Italy
[f]INFN-CNAF, Viale B. Pichat 6/2, Bologna, Italy
[g]LAM, 38 Rue Frédéric Joliot Curie, Marseille, France
[h]Aix-Marseille Université, CNRS/IN2P3, CPPM, Marseille, France
[i]IRAP, 9 Av. du Colonel Roche, Toulouse, France
[j]IPNL, 4 Rue Enrico Fermi, Villeurbanne Cedex, Lyon, France
[k]IP2I, 4 Rue Enrico Fermi, Villeurbanne, France
[l]MPE, Gießenbachstraße 1, Garching Baviera, Germany
[m]NASA, USA
[n]European Space Agency/ESTEC

ABSTRACT

ESA's mission Euclid while undertaking its final integration stage is fully qualified. Euclid will perform an extra galactic survey (0<z<2) using visible and near-infrared light. To detect the infrared radiation is equipped with the Near Infrared Spectro-Photometer (NISP) instrument with a sensitivity in the 0.9-2 µm range. We present an illustration of the NISP Data Processing Unit's Application Software, highlighting the experimental process to obtain the final parametrization of the on-board processing of data produced by an array of 16 Teledyne's HAWAII-2RG (HgCdTe) - each of 2048×2048 px^2, 0.3 arcsec/px, 18 µm pixel pitch; using data from the latest test campaigns done with the flight configuration hardware - complete optical system (Korsh anastigmat telescope), detectors array (0.56 deg^2 firld of view) and readout systems (16 Digital Control Units and Sidecar ASICs). Also, we show the outstanding Spectrometric (using a Blue and two Red Grisms) and Photometric (using Y_E 0.92-1.15µm, J_E 1.15-1.37µm, and H_E 1.37-2.0 µm filters) performances of the NISP detector derived from the end-to-end payload module test campaign at FOCAL 5 - CSL; among them the Photometric Point Spread Function (PSF) determination, and the Spectroscopic dispersion verification. Also the performances of the on-board processing are presented. Then, we describe the solution of a major issue found during this final test phase that put NISP in the critical path. We will describe how the problem was eventually understood and solved thanks to an intensive coordinated effort of an independent review team (tiger team lead by ESA) and a team of NISP experts from the Euclid Consortium. An extended PLM level campaign in ambient in Liege and a dedicated test campaign conducted in Marseille on the NISP EQM model, with both industrial and managerial support,

Further author information: (Send correspondence to)
E-mail: eduardo.medinaceli@inaf.it, Telephone: (+39) 0516398698

finally confirmed the correctness of the diagnosis of the problem. Finally, the Euclid's survey is presented (14000 deg^2 wide survey, and $\sim$40 deg^2 deep-survey) as well as the global statistics for a mission lifetime of 6 years ($\sim$1.5 billion Galaxy's shapes, and $\sim$50 million Galaxy's spectra).

Keywords: Near-infrared, infrared spectrometry, infrared photometry, NISP, Euclid, Application Software

1. INTRODUCTION, THE EUCLID MISSION

Euclid is an ESA mission that will fly an extremely sophisticated space telescope to measure the shapes of more than a billion galaxies (with unprecedented levels of observation accuracy), and accurate redshifts (z) of tens of millions of galaxies.

Euclid is a partnership with the Euclid consortium formed by several research institutes across Europe, Thales Alenia Space (TAS-I) and Airbus Defence and Space (ADS) industries, and NASA's Jet Propulsion Lab/Goddard Space Flight center. Euclid's overall mass is about 2020 Kg having a power consumption of 1920 W, 4.5 m tall and 3.1 m of diameter. It is equipped with a telescope with a primary aperture of 1.2 m, and 2 instruments. The visible imager (VIS) is sensitive to $0.5-0.9$ μm and the Near Infrared Spectro-Photometer (NISP) is sensitive to $0.9-2$ μm, both using a common field of view (FoV). The Euclid satellite has two antennas: X/X (8.2 GHz) and K-band (25.5-27 GHz) with a ground station down-link rate of 55 Mbits/s (850 Gbit/day transferred 4h/day). Fig. 1 shows the integrated flight model at TAS-I premises.

Euclid will perform it's main survey of 15000 deg^2 + 40 deg^2 of deep survey in the halo orbit around the Lagrangian point Sun-Earth (L2), in 6.25 years (plus additional survey). Dark energy is Euclid's main science driver i.e., understanding the acceleration of the Universe.

Figure 1. Euclid's fully integrated flight model, picture courtesy of Thales Alenia Space - Italy.

2. SCIENCE OBJECTIVES

The main science objectives are to measure the expansion history H(z) to high accuracy, as to detect percent variations of the dark energy equation of state with robust control of the systematics, i.e. verify the dynamics of the dark matter evolution. Euclid will measure this using two probes: the scale of Baryonic Acoustic Oscillations (BAO) in the clustering pattern of galaxies as a standard rod; by measuring the spectroscopic redshifts of 50 million galaxies in the redshift range $0.7<z<2.1$ the three dimensional galaxy distribution of the Universe can be mapped to high precision.[1] And using shape distortions induced by weak gravitational lensing; by measuring the correlations in the shapes of the 1.5 billion galaxies, the expansion and growth history of the Universe can be determined with high precision.[1]

Another objective is to measure at the same time the growth rate of structures from the same probes, to detect deviations from general relativity with a very high sensitivity. Using clustering redshift-space distortions, and weak lensing tomography (3D view measuring the z of background galaxies).

3. WIDE SURVEY

A *panchromatic view* strategy is used for the observations of the same FoV using complementary measurements in the visible band (with the VIS detector) and with both photometric and spectrometric images in the infrared band (with the NISP detector). Each single Euclid observation is composed of a visible image and single spectrometric image, followed by 3 photometric images with a total duration of 1 hour and 15 seconds. The daily budget is $\sim$ 20 observations.

The *Dithering technique* is used to correct instrumental effects on the images, to do so, a series of 4 observational sequences (composed as described before) are performed. Each observation is done after a slight change in the telescope pointing (Dither slew). Euclid's reference observational sequence (ROS) is constitute of 4 single observational sequences where the 4^{th} sequence includes a dark photometric exposure.

The complete sequence is build as follows, where the Filter Wheel position is represented with FWA, the Grism Wheel position with GWA and the exposure number with Exp*:
Dither1: Exp1: FWA=Open, GWA=RGS0; Exp2: FWA=J, GWA=Open; Exp3: FWA=H, GWA=Open; Exp4: FWA=Y, GWA=Open.
Dither2: Exp1: FWA=Open, GWA=RG180+4; Exp2: FWA=J, GWA=Open; Exp3: FWA=H, GWA=Open; Exp4: FWA=Y, GWA=Open.
Dither3: Exp1: FWA=Open, GWA=RG0-4; Exp2: FWA=J, GWA=Open; Exp3: FWA=H, GWA=Open; Exp4: FWA=Y, GWA=Open.
Dither4: Exp1: FWA=Open, GWA=RG180; Exp2: FWA=J, GWA=Open; Exp3: FWA=H, GWA=Open; Exp4: FWA=Y, GWA=Open; Exp5: FWA=Open, GWA=RGS0.

4. EUCLID INSTRUMENTATION

Euclid's complete telescope (structure and mirrors) is made of sintered silicon carbide (SiC) that combines a high stiffness, low density, and high thermal conductivity, thus reducing thermal gradients along and across the optical path. The telescope has a three mirror Korsch configuration with 0.45 deg off-axis field with 1.2 m aperture of the primary mirror, and a secondary mirror of 0.35 m. Together providing a collection area of 1 m^2. Visible and near-infrared observations are done with the same FoV using a dichroic beam-splitter.[2]

VIS (spectral range of $550 - 900$ nm) focal plane is composed of 6x6 CCDs ($e2v$, $12 \times 12 \mu m^2$ $pixels$, 4096×4096 $pixels^2$) with a resolution of 0.1 arcsec/px and a FoV = $0.787x0.709$ deg^2 with a focal length of 24.5 m. Its limiting magnitude is 24.5 for extended sources at 10σ. VIS' data rate is $\leq$ 520 Gb/day.

NISP (spectral range of $0.9 - 2$ μm) focal plane is composed of 4x4 H2RG (HgCdTe) CMOS (e2v, $18 \times 18 \mu m^2$ $pixels$, 2048×2048 $pixels^2$) with a resolution 0.3 arcsec/px and a FoV = 0.55 deg^2 with a focal length of $\sim$6.1 m. NISP's data rate is $\sim$290 Gb/day. For the photometry, the limiting magnitude is 24, and the redshift resolution is $dz/(1+z) = 5\%$; the spectral range is $\Delta\lambda : 920 - 1146$ nm. For the spectroscopy, the limiting magnitude is 19.5. Red-shifted H_α (656 nm) at $z = 0.8 - 1.8$. The redshift resolution is $dz/(1+z) = 0.1\%$, and the spectral range is $\Delta\lambda : 920 - 1850$ nm.

This paper presents the main features and performances of the NISP detector, including the on-board signal pre-processing.

4.1 NEAR-INFRARED SPECTRO-PHOTOMETER, NISP

The Euclid's Spectro-Photometer consists of an opto-mechanical assembly (NI-OMA) and an Infrared Detector Assembly (NI-DA). The NI-OMA includes collimators and focusing lenses mounted on a SiC structure and the NI-DA accommodates the Infrared Detector which is sensitive to photons in the [0.9-2] µm spectral range. Is also equipped with a filter and a grism wheel assembly providing spectrometric and photometric capabilities. Figure 2 shows the components of the NISP detector. On the left-side the optical and mechanical support assemblies are

shown; while on the right-side of the figure the two filter and grism wheel systems are shown. For the photometry NISP uses three filter passbands: Y_E (0.92-1.15µm ± 0.2 nm), J_E (1.15-1.37µm ± 0.3 nm), and H_E (1.37-2.0 µm ± 0.4 nm)[3] represented in fig. 3. While, for the slitless spectroscopy NISP uses 4 grisms: one blue (920-1400 nm) with single orientation of 0°, and 3 red (1200-1950 nm)[3] with orientations 0°, 90° and 180° also represented in the same fig. 3.

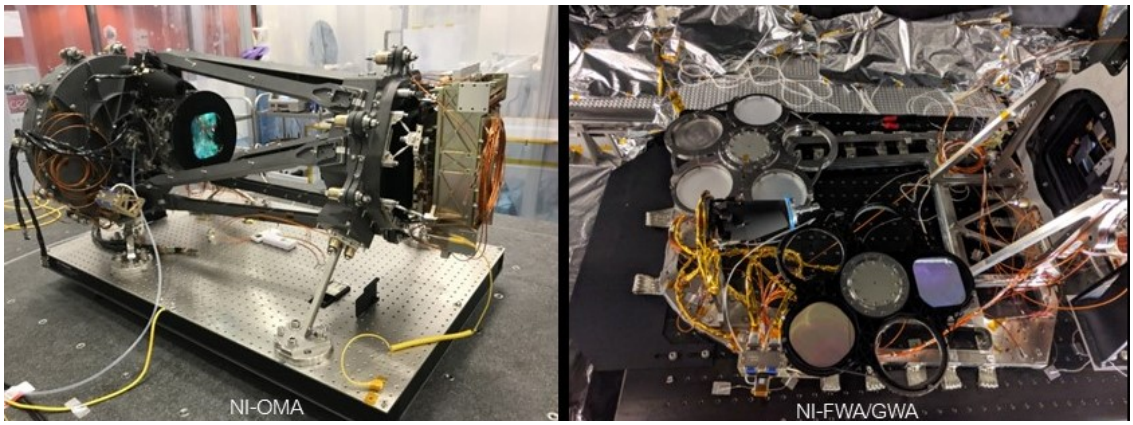

Figure 2. *Left:* NISP detector in its final configuration. Only the collimator lens is visible (the focusing one in the opposite position is not); the wheels' container structure can be seen on the far left, and the focal plane on the far right. The complete system is sustained by a SiC structure. *Right:* both filter wheel (top) and grism wheel (bottom) in a horizontal position during the LAM test setup. The calibration unit is also visible at the center of the image.

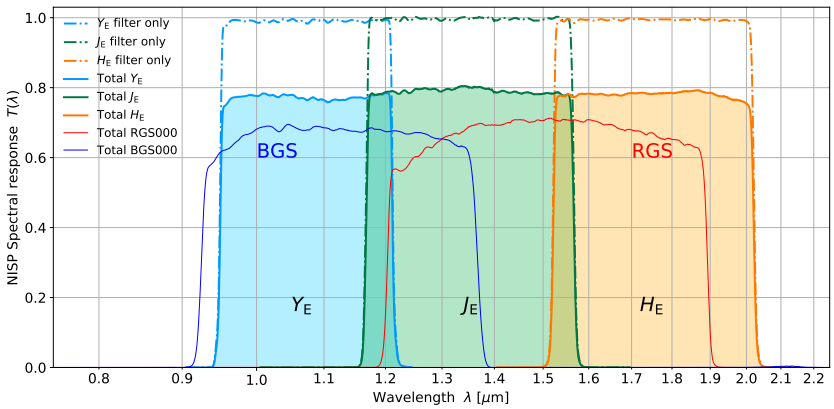

Figure 3. NISP transmission elements. The thin lines show the effective filter transmission integrated over the beam footprint, and the shaded areas the total response. Total RGS000 and BGS000 grisms spectral response are plotted with solid lines.[3]

The NISP detector system is composed of an array of 4x4 HAWAII-2RG sensors from Teledyne Imaging Scientific, each one is an array of 2028x2048 px^2 operated at ∼90 K. A molybdenum (10.2 g/cm^3) mechanical structure holds the detectors and a burnished aluminum (2.7 g/cm^3) truss holds the 16 SIDECAR ASICs (operating at ∼135 K), this structure can be seen at the right-side in both images of fig. 2. In the same figure the focal plane array is partially visible on the right-side.

The detector system is controlled by two identical Data Processing Units (DPU) performing synchronous operations, each one controlling half focal plane. Each DPU is equipped with 8 Digital Control Units (DCUs) each one interfaced with an ASIC. DPUs are commanded by the Instrument Control Unit (ICU) which receives the telecommands from the s/c. The DPU telemetry is collected by the ICU, packetized and sent to the S/C.

The ICU monitors some selected DPU parameters to trigger Instrument level FDIRs and other events (e.g.: end of exposure, end of transmission). The system so-called warm electronics, operate at Spacecraft's service module at ∼293 K; see the scheme of figure 4.

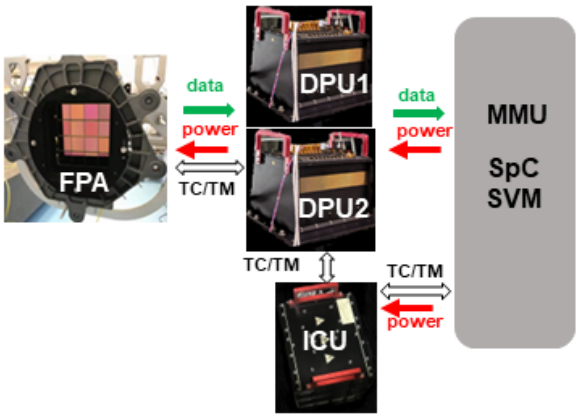

Figure 4. Scheme of NISP main communication and power interfaces. The NISP warm electronics is composed of two identical Data Processing Units (DPU1 and DPU2 shown at the center of the scheme). They control the NISP focal plane (FPA, shown at the left-side). DPUs are commanded by the Instrument Control Unit (ICU shown at the bottom) that is interfaced with the Spacecraft's service module (SpC SVM, represented on the right-side of the scheme). White arrows represents the commandability and telemetry retrieval flux - using a MILBUS1553 link, green arrows shows the science data flux stored on the SpC's Mass Memory Unit (MMU), using a SpaceWire interface. Red arrows represent the power distribution provided by the SpC. A picture of the NI-WE components can be seen also on the left-side of fig. 8.

4.2 NISP ON-BOARD PROCESSING

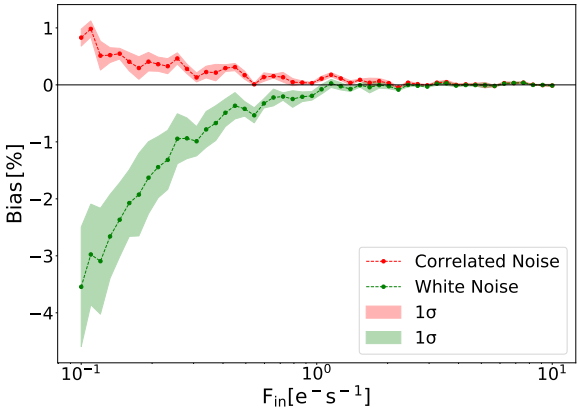

Figure 5. Reconstructed flux estimation bias as a function of the flux. Two approximations are shown, correlated noise (pink) and white noise (green). Both models provides an almost null (∼0.1%) bias for a flux in the region of Euclid's sky observations i.e. higher than (1-2 e/s).[4]

The DPU application software (ASW) architecture is driven by the science performances, operating and controlling dedicated electronics suited to cope with the time constraints of the NISP acquisition sequences during the sky survey. The same DPU-ASW running in both DPUs implements a multi-task preemptive scheduling algorithm written in ansi-C (ECSS standards) running in a VxWorks 5.1 real-time operative system. With 13 tasks it handles the spacecraft's time distribution and the synchronization of all the subsystems with a frequency of 1 Hz, a command rate ∼512 bit (1 Hz), a telemetry rate ∼18 kbits (40 Hz), and a science data production of ∼290 Gbit/day. The main task of the DPU-ASW is the implementation of the on-board pipe-line allowing

all basic operations to evaluate the signal acquired using the multi-accumulation charge collection (MACC) technique. The processing includes the up-the-ramp input exposure frames being averaged in groups, where the signal estimation is obtained with a weighted least-square fit of the charge derivatives. A quality statistical estimator of the fit is evaluated (χ^2, with different resolutions for each exposure mode i.e. spectrometric using 16 bit/px or photometric using 1 bit/px). The on-board processing algoirthm is executed recursively for of all the 16 detector (8 per DPU), considering for each detector every single sensitive pixel (2040×2040 px^2). An array of 4×4 px^2 is used to correct the image by the thermal background noise. The DPU-ASW performs a data-volume compression before the ground down-link.[5] The on-board processing algorithm depends on two

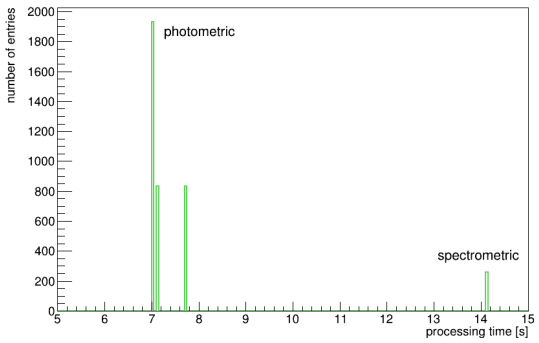

Figure 6. NISP Data processing Unit performances - on-board processing time. The time depends on the acquisition type i.e. spectrometric (spectro) using 15 co-added frames for the linear fit, or photometric (photo) using 4 groups. The mean processing times (TV3 dataset) are ∼ 7.1 s for photometric data, while ∼ 14.1 s for spectrometric acquisitions. Both have standard deviations below 0.1s. The second peak in the photometric distribution comes from data with a test processing configuration.

main parameters (personalized for each detector), i.e. the detector's read-out-noise (RON) and the gain. The correlated RON (which includes the Poissonian photon noise) is approximated by the white noise approximation[6] and is Gaussian distributed in the time domain. As demonstrated in[4] there is no bias introduced - differences lower than ∼ 0.1 % - by the Gaussian assumption (white noise) implemented in the on-board processing for Euclid's sky observations (1-2 e/s), as shown in figure 5. Detector's gain may be considered as the combination of two terms: the charge-to-voltage conversion (V/e^-) and the analog-to-digital conversion (ADU/V). The RON and the gain for each detector were obtained experimentally during a dedicated characterization test campaigns (TV1/TV2, section 5). The following results were obtained using the final detector's parametrization. The processing time of spectrometric and photometric acquisitions were derived from the data of the latest test campaigns being ∼14 s and ∼7 s respectively, see the distributions of figure 6. Another result is the size of the NISP data products, which depends on the results of the on-board compression algorithm; a loss-less compression algorithm (NASA CFITSIO) is implemented in the DPU-ASW, and its performances depends on the acquisition type. In figure 7 are shown the signal (*left*) and χ^2 (*right*) compression factors (CF, defined as the ratio of the compressed and original frame sizes) obtained during NISP performances tests. In the plot the mean values $CF_{spectro\ science} = 2.85$, $CF_{photo\ science} = 3.4$, $CF_{spectro\ \chi^2} = 1.15$ and $CF_{spectro\ \chi^2} = 2.2$ are indicated with dashed horizontal lines. Each detector data product (transmitted separately) is composed of the science frame, the χ^2 frame, a header, and a set of telemetry; and the mean size of a nominal NISP single dither sequence (full FPA), see section 3, is 379.2 MByte. Then, assuming 20 cycles per day of reference observation cycles the data produced amounts to 26.3 GByte/day.

5. NISP TEST CAMPAIGNS

NISP was extensively tested at the *Laboratoire d'Astrophysique di Marseille (LAM)* France, in different sessions; the setup is shown in the left-side of figure 8. In the thermal vacuum and thermal balance (TBTV) TV1/2 test campaign the detectors were fully characterized and a personalized parametrization to optimize the throughput of each single detector was obtained. Afterwards, in the TV3 test campaign, the optical system and the detector

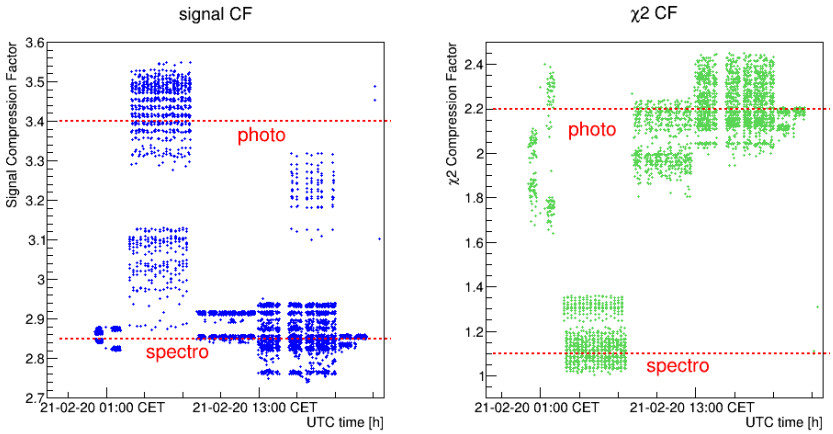

Figure 7. Data Processing Unit on-board processing performances. Compression Factor (CF) of ∼4000 processed images and χ^2 frames. Results are different for spectrometric (labelled spectro) and photometric (labelled photo) datasets, the horizontal lines indicates the mean values. *Left-side*: science frames results: spectro CF = 2.85, photo CF = 3.4. *Right-side*: χ^2 frames results: spectro χ^2 CF = 1.15 , photo χ^2 CF = 2.2.

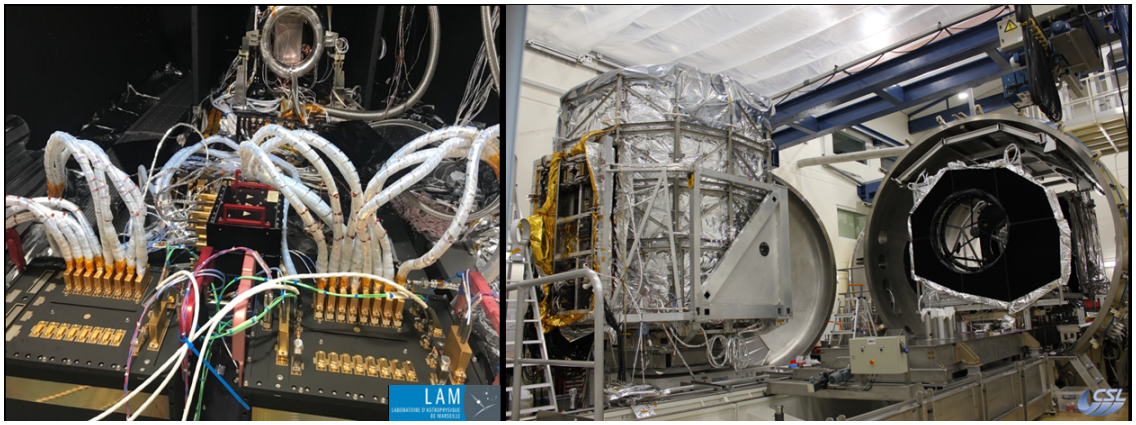

Figure 8. *Left*: NISP tests setup at *Laboratoire d'Astrophysique di Marseille*, France. NISP warm electronics close-up, from bottom to top: the two DPUs, the ICU, and the focal plane array. *Right*: Euclid's end-to-end PLM test setup at the *Centre Spatial de Liège*, Belgium. The NISP warm electronics mounted on the pannel Y can be seen at the left-side of the picture (vertical structure partially covered with MLI), and the telescope placed horizontally at the right-side of the image.

performances were evaluated. This session last ∼3 months, and ∼40K commands were executed, ∼19K images per detector were acquired, ∼300K files were produced, and a continuous run of 72h of wide survey were exercised. In this test campaign the NISP focus was determined, as well as the instrument dark level. The optical quality of grisms (spectrometric) and filters (photometric) were determined by testing the focus. Also the spectral resolution was assessed by testing the dispersion for the red grisms RGS000, RGS180 and blue grism BGS000. Also the requirements of the signal-to-noise ratio for the spectroscopy with RGS000, RGS180, and BGS000, and for the photometry with Y, J and H bands were verified *.

In 2021 during the Euclid's end-to-end PLM test campaign both NISP and VIS instruments were integrated with the telescope, and global performances were derived. The campaign was carried out at the *Centre Spatial de Liège* (CSL), Belgium by ADS and took 1 month of nominal continuous operations at TBTV. The setup can be seen in the picture of the right of figure 8. At CSL the NISP/VIS auto-compatibility (cross talk) was tested

*more details in Paper 12180-57 of this proceedings

demonstrating that the instruments were not interfering, and the NISP/VIS common focus was obtained. For NISP the reference dark level was obtained, as well as the photometric and spectrometric point spread functions (PSF), and the spectroscopic dispersion was verified. NISP's photometric PSF and the spectrometric dispersion are presented in section 6.

5.1 Major issue during PLM test campaign

Only 7 out of 16 NISP detectors worked correctly during the CSL campaign at cryogenic conditions (FPA temperature ∼90K). In some of the 9 non-working detectors 'artifacts' were present on the science images i.e., horizontal or vertical patterns, and all 9 stopped producing data after the first exposure. This anomalous behaviour was not present at CSL during the reference tests at room temperature using the same hardware configuration, neither on the cryogenic tests at LAM using the same flight hardware. Despite this limitation, Euclid's optical performances (listed in section 5) could be verified using correctly operating detectors, placed both at the edge and at the center of the NISP FPA.

A huge troubleshooting strategy was defined to address this issue. Including an external ESA team of experts to scrutinize the NISP operations; brainstorming with the detector and readout electronics provider (NASA), and DPU hardware provider (OHB-I). Industrial partners (TASI and ADS) perform indipendent analysis, and look for possible external factors coming from the test facility. The only difference found at the CSL setup with respect to LAM setup was the introduction of extension harnesses connecting the FPA with the DCUs of the DPUs. To characterize the electrical signals between the front-end electronics (sidecar ASICs) and the Digital Control Units (details in section 4.1) two new dedicated test campaigns were set in place. In this interface errors were triggered during the test campaign. The first campaign was an extension of the PLM tests at warm ambient conditions at CSL. The data there was used as reference because in this conditions there were no errors generated. Then a completely new cryogenic test campaign at LAM was set using the Electrical Qualification Models of the WE. Signal electrical characterization at LAM was done using the hardware configuration shown in figure 9, the nominal components of the connection harness between a single DCU and an ASIC (labelled SCE - sensor chip electronics) composed of different segments in the cold section inside the thermal vacuum cryostat (TGS, CIS and Flex) are shown; as well as the components outside the cryostat (at room temperature) i.e. the extension harness and an adjustable delay line (labelled test-aid). Electrical measurements were done accessing the signal through an *ad-hoc* break-out box (JIG). Differences in the transmission time for some detectors in the CSL

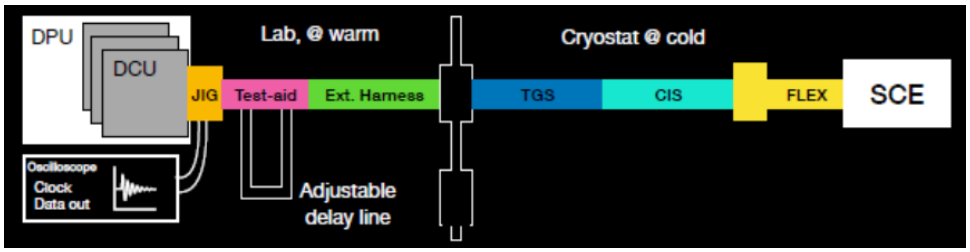

Figure 9. Cryogenic test setup used at LAM. The different segments (inside and outsithe the cryostat) of the connection harness between the DCU and the ASIC (SCE) are shown. The test-aid (delay line) allows to inject an adjustable delay in the signal propagation, and digital signals were accessible through the the break-out box (JIG).

configuration of the order of ∼ns were found. Then, the CSL error condition was reproduced varying the cable lengths by some ∼cm, i.e. inducing a delay in the signal propagation generating errors and the stop of the nominal operations. The width of the delay window causing the errors was of 3ns. The ESA team pointed out a non correct treatment of these errors. Analyzing the induced errors an inconsistency in the hardware documentation leading to an incorrect DCU-ASIC I/F error treatment implemented in the DPU-ASW was found. A native double sampling strategy (using two FIFOs) implemented in the DCU drivers was injecting false positive errors when the signal was sampled outside an acceptance window of one of the FIFOs, even if the transmission was correctly recovered by the other FIFO. The false positives were interpreted by the software as true errors and all the science interface was reset causing the stop of the data production. The issue was corrected implementing a new comprehensive error strategy handling the DCU-ASIC interface in the DPU application software.

6. EXAMPLES OF NISP PERFORMANCES

Some of the NISP performances results obtained during the system level tests done at the facilities described in section 5 are presented.

6.1 NISP Photometric PSF evolution

The PSF determination was done using a single long exposition, and because NISP's sub-pixel size of the PSF, 25 PSF flashes (grid of 5x5) at different locations were done using a monochromatic point-like source. Figure 10 shown the photon counts obtained for the blue grism BGS000 (on the left-side), for the red grism RGS000 (center), and for the RGS180 (right-side). The collimator was at warm temperature, therefore was emitting thermal radiation and the background present special features at small scale; the background flux increasing with the wavelength. This introduced a large background during the PSF characterization for the red grism at CLS. This effect was included in the model of the PSF determination. The PSF is modelled by a 2D asymmetric

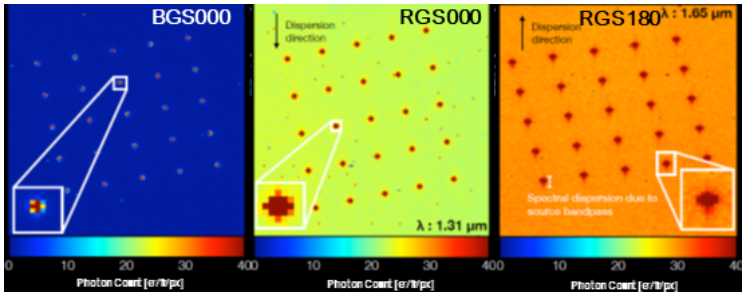

Figure 10. NISP photometric PSF determination. Images show the 25 PSF acquisitions done with the M2M mirror at NISP/VIS best focus position during the CSL test campaign. The image on the left-side correspond to the blue grism BGS000, while the images on the center and on the right-side are for the red grism with the RGS000 and RGS180 orientations respectively. Image courtesy of W. Gillard - CPPM.

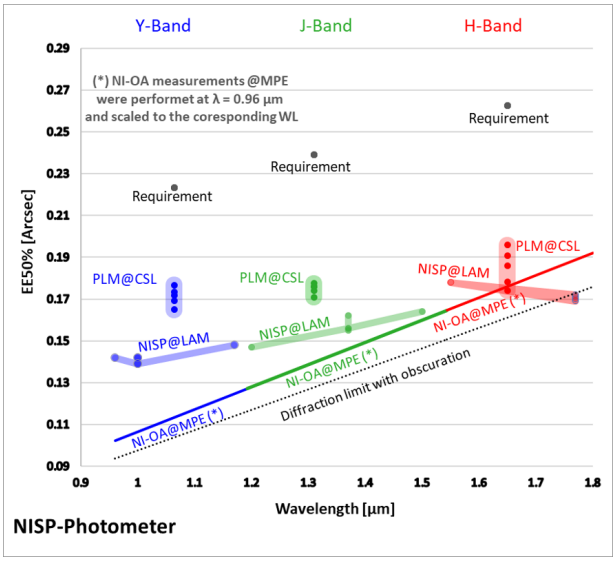

Figure 11. Evolution of the diffractive EE50 radius vs. wavelength. NISP (LAM) and end-to-end (CSL) results for the Y, J and H bands are plotted with blue, green and red markers respectively. Stable values are well below the requirements (with black markers), and are near to the diffraction limit (dashed line). Reference measurements done with NISP optical system stand-alone (NISP-OA@MPE) are also included. Image courtesy of F. Grupp - MPE.

Erf funcion considering a Gaussian pixel integration, and the 50% Encircled Energy radius EE50 was deduced

from the width of the Gaussian (centroid position of the PSF that contains the 50% of the total PSF's energy). CSL results are compared with the ones obtained during NISP tests at LAM in figure 11. In the figure can be seen that the EE50 for the different photometric bands is very stable, with median/mean values below the requirement (< 40%) indicated with black dots, and close to the theoretical limit (indicated with the dashed line - diffraction limit with obscuration).

6.2 NISP Spectrometric dispersion verification

Also in this case the spectrometric calibration was verified using the results from the NISP-TV3 test campaign at LAM with the end-to-end tests done at CSL. The NISP Optical Ground Equipment used during TV3 was used to verify the spectral dispersion at PLM level. During both test campaigns the same spectral source was used i.e., etalon. The etalon is a 55 μm air-space Fabry-Perot interferometer providing 34 transmission peaks in the NISP's red-grism band pass. Figure 12 shows the comparison between the two spetra obtained with the RGS000. For the comparison no rotation, neither stretching was applied, only a solid translation of the 0^{th} order was added to manually align each other. The figure shows almost a perfect match between the RGS000 spectra from TV3 (contour) and PLM spectra (color). The overall dispersion-distance between the Fabry-Perot peak

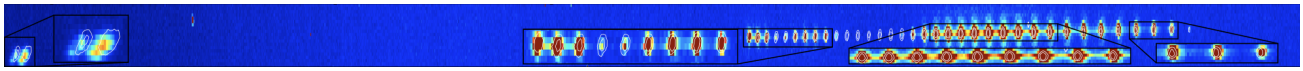

Figure 12. Red-grism RGS000's Fabry-Perot peak position comparison of the spectra obtained at the NISP-TV3 tests (LAM), and the end-to-end tests (CSL). Tv3 spectra is plotted with a contour scale, while PLM spectra with a color scale. An almost perfect match was obtained, on the *left-side* the 0^{th} order is shown, and on the *rigth-side* the 1^{st} order. Inside the black boxes shows are shown the zoom-in of parts of the spectrums. Image courtesy of W. Gillard - CPPM.

position measured at TV3 and PLM are well below (40%) the requirement, amounting to < 0.8px giving no significant impact of dichroic on the dispersion solution. The results for the projection of the focal plane axis y and z for the BGS000, RGS000 and RGS180 are shown in figure 13; for each case the mean values (bias) and the standard deviation are quoted.

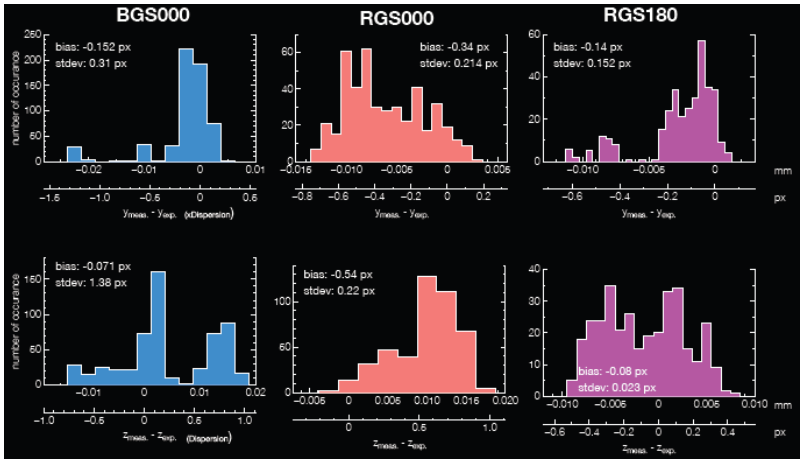

Figure 13. Comparison of the distance-dispersion of the TV3 spectra (y_{exp} (top row) and z_{exp} (bottom row)) with the PLM data. The mean values (bias) and the standard deviation (stdev) are presented for the BGS000, RGS000 and RGS180 grisms. The deviations are within the requirement (< 0.8) px. Image courtesy of W. Gillard - CPPM.

7. EUCLID SURVEY

Euclid's survey strategy is based in a step-and-stare mode imaging with a FoV $\sim 0.5\ deg^2$. The line spacecraft-Sun moves 1 degree/day over the ecliptic plane and the daily base coverage is of 15-20 degrees. Figure 14 shows

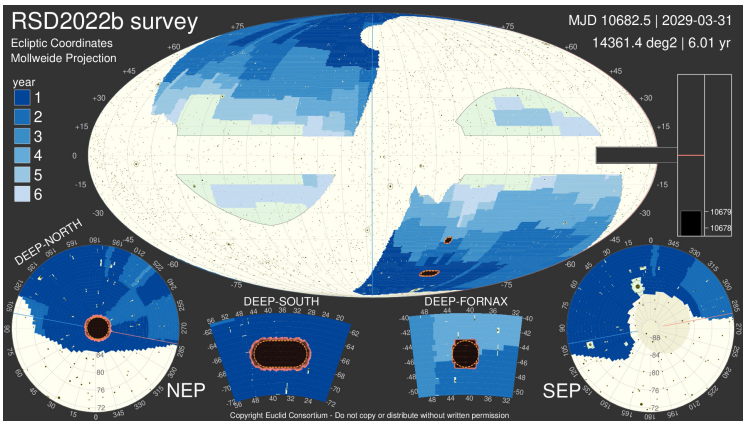

Figure 14. Euclid's survey (version RSD2020b of 12/31/2022) after 6 years of mission lifetime represented in ecliptic coordinates using the Mollweide projection. The wide survey (15000 deg^2) is plotted using a blue color scale, are also shown the 4 regions (NEP, DEEP-SOUTH, FORNAX and SEP) of the deep-survey ($\sim$40 deg^2). The exclusion zones are represented with a white area. Image courtesy of J. Dinis - Faculdade de Ciências da Universidade de Lisboa.

Euclid's global wide survey (represented with a blue color scale) coverage of 14000 deg^2 of extra-galactic sky with more than 40000 observations obtained during the mission lifetime of $\sim$6 years, which is more than 35% of the celestial sphere. Euclid will measure the shapes of $\sim$1.5 billion Galaxies (weak lensig) and the spectra of $\sim$50 million Galaxies (red-shifts). Euclid will also perform a deep-survey with $\sim$2 higher magnitudes than the Wide-survey over an area of $\sim$ 40 deg^2 made in 4 regions of 10 deg^2 (DEEP-NORTH, DEEP-SOUTH, DEEP-FORNAX and SEP) shown in the same figure. The exclusion zones are $\pm 25°$ Galactic plane latitude to avoid stellar contamination, and $\pm 15°$ Ecliptic plane latitude to avoid zodiac light contamination, represented in the same figure with white regions. Euclid will measure the shapes of 50000 Galaxies/field leading to 1.5 billion Galaxies and the spectra of 850 Galaxies/field leading to a total of 25 million Galaxy spectrums.

REFERENCES

[1] R. L. et al., "Euclid mapping the geometry of the dark universe," *Definition Study Report ESA/SRE(2011)12* , 2011.

[2] L. M. G. V. et al., "Euclid payload module : telescope characteristics and technical challenges," in *Space Telescopes and Instrumentation 2014: Optical, Infrared, and Millimeter Wave*, *Proc. SPIE* **9143, id. 91430I**, 2014.

[3] E. collaboration: M. Schirmer et al., "Euclid preparation. xiii. the nisp photometric system," *Astronomy Astrophysics* **662, A92**, 2022.

[4] A. J. M. et al., "Euclid: Estimation of the impact of correlated readout noise for flux measurements with the euclid nisp instrument," *The Astronomical Society of the Pacific* **133 (1027)**, 2021.

[5] C. B. et al., "On-board data processing for the near infrared spectrograph and photometer instrument (nisp) of the euclid mission," in *Space Telescopes and Instrumentation 2016: Optical, Infrared, and Millimeter Wave*, *Proc. SPIE* **9904, id. 99045R 11 pp.**, 2016.

[6] B. K. et al., "A new signal estimator from the nir detectors of the euclid mission," *The Astronomical Society of the Pacific* **128, n.968**, 2016.